

# Synthesis, structural and DFT interpretation of a Schiff base assisted Mn(III) derivative

Kuheli Das <sup>a, \*\*</sup>, Chiara Massera <sup>b</sup>, Eugenio Garribba <sup>c</sup>, Antonio Frontera <sup>d</sup>, Amitabha Datta <sup>e, \*</sup>

<sup>a</sup> Department of Chemistry, University of Calcutta, 92 A.P.C. Road, Kolkata, 700009, India

<sup>b</sup> Dipartimento di Scienze Chimiche, della Vita e della Sostenibilità Ambientale, Università degli Studi di Parma, Viale delle Scienze 17/A, 43124, Parma, Italy

<sup>c</sup> Dipartimento di Chimica e Farmacia, Università di Sassari, Via Vienna 2, I-07100, Sassari, Italy

<sup>d</sup> Departament de Química, Universitat de les Illes Balears, Ctra de Valldemossa km 7.5, 07122, Palma de Mallorca, Baleares, Spain

<sup>e</sup> Institute of Chemistry, Academia Sinica, Nankang, Taipei, 115, Taiwan

## ARTICLE INFO

### Article history:

Received 9 April 2019

Received in revised form

19 August 2019

Accepted 25 August 2019

Available online 26 August 2019

### Keywords:

Mn(III)

Schiff base

Crystal structure

EPR

DFT

## ABSTRACT

A mononuclear Mn<sup>III</sup> derivative, [Mn(L)(SCN)(H<sub>2</sub>O)] (1) [where H<sub>2</sub>L = *N,N'*-bis(salicyldehydene)-1,3-diaminopropan-2-ol] has been synthesized and systematically characterized. In 1, the central Mn<sup>III</sup> ion is linked to the NNOO donor atoms of the potentially binucleating precursor L<sup>2-</sup> and additionally coordinates one water molecule and the pseudohalide SCN<sup>-</sup>, thus yielding a distorted octahedral geometry. The UV-Vis spectra of 1 shows an intense band corresponding to a <sup>5</sup>T<sub>2g</sub> - <sup>5</sup>E<sub>g</sub> transition at 545 nm; thus presuming the octahedral geometry around the Mn ion. The solid and solution EPR spectra of 1 have been simulated with an HP 53150A microwave frequency counter which has confirmed the +3 oxidation state of the metal ion. We have also conducted a DFT computational study which has confirmed that compound 1 self assembles into a two-dimensional network via O-H···O, π-π, and unconventional C-H ... π(SCN) interactions involving the π-system of the thiocyanate. The room temperature magnetic susceptibility of compound 1 has yielded an effective magnetic moment ( $\mu_{eff}$ ) value of 4.96 B.M.

© 2019 Elsevier B.V. All rights reserved.

## 1. Introduction

The rational design and synthesis of new coordination complexes of transition metals and multifunctional bridging ligands is of great research interest, due to their potential applications as functional materials and for the interesting topologies they can create. In this context, substantial research is devoted to the chemistry of manganese complexes with different oxidation states incorporating N,O donor ligands [1–6] of various denticity. Indeed, these ligands can display stereochemical diversity, specifically with respect to their coordination numbers and/or geometry when combined with different transition metals. In this framework, tridentate and tetradeятate precursors like salen-type Schiff bases have been shown to form metal derivatives which can manifest unusual coordination, high thermodynamic stability and kinetic

inertness [7–9]. The geometry of these metal derivatives depends upon the size and electronic configuration of the metal ions, the inherent rigidity of the ligand due to the presence of aromatic rings, the presence of repulsive forces between non-bonded atoms in different ligand arms etc [10–15]. Manganese(III) salen-type complexes are very well studied because this type of Schiff base precursors [16,17] have revealed to be suitable for biological applications [18,19]; besides, structurally diverse derivatives can be good candidates for molecule-based magnetic materials [20–23]. Pseudohalide (OCN<sup>-</sup>, SCN<sup>-</sup>, N3<sup>-</sup>, etc.) ions can coordinate to transition metal atoms in different ways, for example as a terminal or bridging ligands [24]. The crystallographic networks of Mn(III) compounds containing pseudohalides as ligands have also been reported by some groups [25–28]. Finally, Mn(III) compounds incorporating salen-type Schiff base precursors with ancillary N-donor co-ligands show interesting structural diversity and topological features [29–34]. In this context, we [35–41] and other groups [42–47] have reported a large variety of metal complexes with tridentate (N<sub>2</sub>O donor) and tetradeятate (N<sub>2</sub>O<sub>2</sub> donor) Schiff base precursors. These studies have demonstrated the role played

\* Corresponding author.

\*\* Corresponding author.

E-mail addresses: [kuheli.chemistry@gmail.com](mailto:kuheli.chemistry@gmail.com) (K. Das), [\(A. Datta\).](mailto:amitd_ju@yahoo.co.in)



by the different transition metal ions and the Schiff base ligands in the formation of coordination motifs with different nuclearities, dimensionalities and topologies. Employing the precursor, [salicylalidimine ligand system], before several articles are published mainly on Cu<sup>II</sup>, Co<sup>II</sup> and Ni<sup>II</sup> metal ions; but there is no report of the Mn-derivative coupled with same precursor and pseudohalide (-SCN) alongwith DFT interpretation till date. In the present contribution, we have employed a potentially N,O-donor Schiff base precursor, which, however, uses four coordination sites (NNOO) to afford a new Mn(III) derivative, [Mn(L)(SCN)(H<sub>2</sub>O)] (1) [where H<sub>2</sub>L = C<sub>6</sub>H<sub>4</sub>(OH)-CH=N(CH<sub>2</sub>)-CH(OH)-(CH<sub>2</sub>)N=CH-(OH)C<sub>6</sub>H<sub>4</sub>] [48]. We have carried out a systematic investigation of complex 1 by means of different spectroscopic measurements. Density functional theory calculations have been used to assess the structural optimization of the compound and have been conducted in combination with MEP and NCI plots to explain the self-assembly of 1 into a two-dimensional network that rationalizes the energetically most-favoured conformations.

## 2. Results & discussion

### 2.1. Synthesis and characterization

The Schiff base precursor, H<sub>2</sub>L [where H<sub>2</sub>L = N,N'-bis(salicylaldehyde)-1,3-diaminopropan-2-ol] is a condensed product of salicylaldehyde and 1,3-diamino-2-propanol [48]. The stoichiometric reaction of H<sub>2</sub>L, MnCl<sub>2</sub>.4H<sub>2</sub>O and NaSCN in a methanol/water mixture affords compound 1 in moderate yield (see Scheme 1), in which the Mn(II) ion has undergone an oxidation to Mn(III). The FTIR spectrum of compound 1 has been analyzed in comparison with that of the respective free Schiff base ligand in the region 3600–450 cm<sup>-1</sup> and it shows data consistent with the structure of the metal derivative.

The absence of a weak broad band, observed in the region of 3600–3400 cm<sup>-1</sup> due to OH<sub>phenolic</sub> absorption of the free Schiff base precursor, agrees with the formation of a new C–O absorption band after complexation with the metal center, as the ligand undergoes deprotonation [49]. The v<sub>C=N</sub> band, appearing at 1611 cm<sup>-1</sup> in 1, indicates that the azomethine nitrogen atom is coordinated by the metal center [50–52], since for the free ligand, the same band is found at 1690 cm<sup>-1</sup>. Besides, the strong band at 2057 cm<sup>-1</sup> corresponds to the stretching vibration of the N-coordinated –SCN moiety. The water molecule coordinated by the Mn(III) ion displays a broad band at 3321 cm<sup>-1</sup>. The ligand coordination to the metal centre is further substantiated by the band appearing at 455 cm<sup>-1</sup> which is mainly attributed to a v<sub>M-N</sub> stretching frequency. Finally, the single-crystal X-ray diffraction analysis has confirmed that the resulting compound is a mononuclear octahedral Mn(III) derivative.

### 2.2. Crystal structure

The molecular structure of 1 consists of a mononuclear

compound of general formula [Mn(L)(NCS)(H<sub>2</sub>O)], where H<sub>2</sub>L is N,N'-bis(salicylaldehyde)-1,3-diaminopropan-2-ol. The compound crystallizes in the monoclinic space group C2/c, and its asymmetric unit is shown in Fig. 1. The Mn(III) ion shows a distorted octahedral geometry of the type O3N3, where the deprotonated ligand chelates the metal through two O and two N atoms, while a water molecule and a thiocyanate ion occupy the two remaining positions (See Table 1 for selected bond distances and angles). The water molecule forms an intramolecular H-bond with the oxygen atom O1 of the ligand. In the lattice, the complexes are connected through a network of hydrogen bonds involving the coordinated water molecule O1W and the hydroxyl group O1-H1 (see Table 2 and Fig. 2).

In particular, a double, centrosymmetric ribbon is formed along the c-axis direction through O1-H1···O2<sup>i</sup> and O1W-H1W···O3<sup>ii</sup> interactions [symmetry codes: (i) = x, -y, -1/2 + z; (ii) = 2-x, y, 3/2-z]. These ribbons are in turn connected in the ab plane through S1···S1 interactions [4.393(3) Å [53], see Fig. 3].

### 2.3. Electronic spectra

The UV–Visible spectrum of compound 1 was recorded using HPLC grade methanol in the range of 200–800 nm. The observed electronic spectral data are in good agreement with the geometry displayed by the compound. The electronic transition bands appear at 215, 233, 279 and 375 nm which may be attributed to π→π\* and n→π\* transitions [54]. In the spectrum, a much weaker, less well-defined broad band is originated in the lower energy regions associated with d–d transitions. Thus, compound 1 is concluded to have an octahedral geometry, showing an intense band corresponding to a <sup>5</sup>T<sub>2g</sub> – <sup>5</sup>E<sub>g</sub> transition at 545 nm; this band specifically indicates the presence of a Mn(III) derivative, comparable to previous data reported in the literature [55–57] (see Fig. 4).

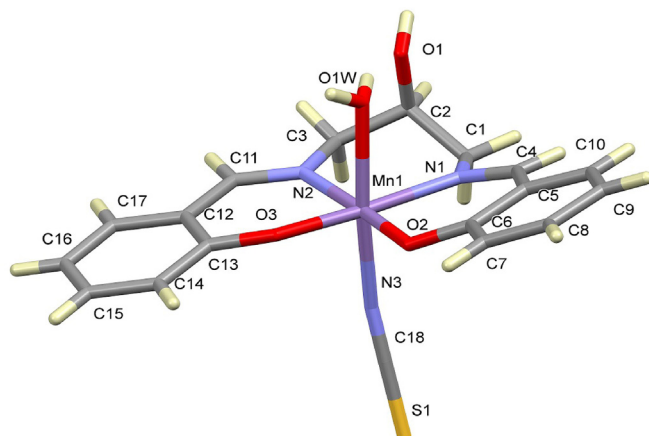
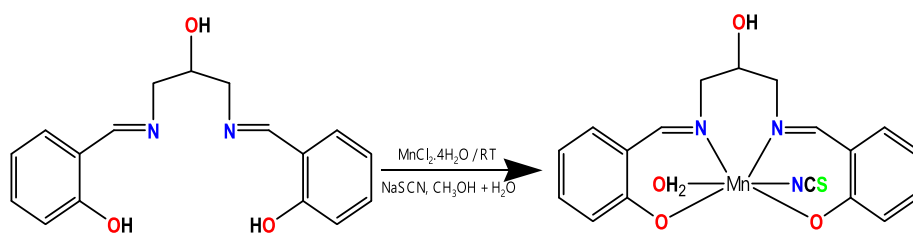


**Fig. 1.** Asymmetric unit of 1 with partial labelling scheme.



**Scheme 1.** Formation of compound 1.

**Table 1**Selected bond lengths [ $\text{\AA}$ ] and angles [ $^\circ$ ] for 1.

Mn1-N1	2.028(3)	Mn1-O1W	2.302(5)
Mn1-N2	2.052(4)	N1-Mn1-O3	171.2(1)
Mn1-O2	1.881(3)	N2-Mn1-O2	174.5 (1)
Mn1-O3	1.898(2)	N3-Mn1-O1W	172.2(2)

**Table 2**Relevant geometrical parameters ( $\text{\AA}$ ,  $^\circ$ ) for the hydrogen bonding network in 1.

D-H···A	D-H	H···A	D···A	D-H···A
O1W-H2W···O1	0.83(9)	2.01(7)	2.808(5)	160(7)
O1-H1···O2 <sup>i</sup>	0.82	2.879(5)	2.882	159
O1W-H1W···O3 <sup>ii</sup>	0.77(5)	2.07(5)	2.803(4)	159(6)

## 2.5. EPR spectra

The EPR spectra on the polycrystalline powder of 1, recorded as a function of the temperature, are reported in Fig. S2 and are silent between 298 and 100 K. However, even if no resonances were revealed while changing temperature, some important findings can be argued. In particular, the lack of signals can be ascribed to the even number of electrons, a situation for which the zero field splitting is usually large, and to the fast relaxation time [59,60]. This indicate an oxidation state +III for Mn, which is generally inactive at the X-band frequency [61]; in contrast, both Mn(II) ( $3d^5$ ) and Mn(IV) ( $3d^3$ ) would give well-resolved spectra even at room temperature [59–61]. Moreover, the results are compatible with those obtained for other Mn(III)-salen compounds for which a  $S = 2$  state

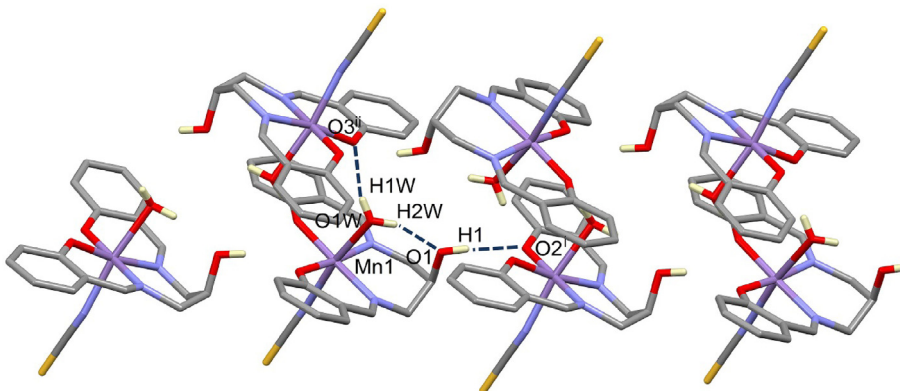


**Fig. 2.** Hydrogen-bonded chains of 1 along the  $c$ -axis direction. Only the H atoms involved in the supramolecular interactions (blue dotted lines) are shown. Symmetry codes: (i) =  $x, -y, -1/2 + z$ ; (ii) =  $2-x, y, 3/2-z$ .

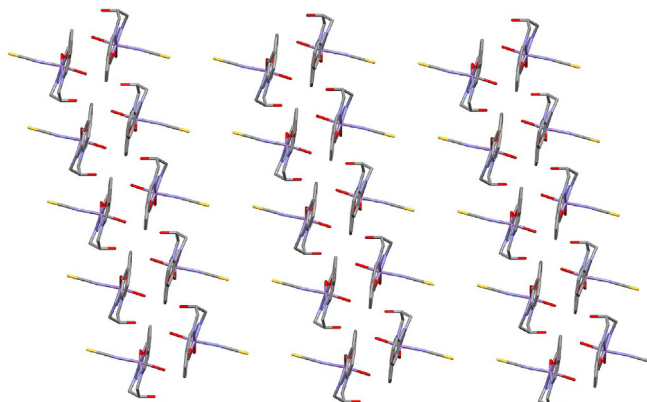


**Fig. 3.** Packing of 1 viewed along the  $b$ -axis direction, in the  $ab$  plane. H atoms have been omitted for clarity.

## 2.4. Magnetic susceptibility

Generally speaking, the magnetic properties of a compound arise from the spin and orbital angular momentum of its electrons. However, the spin-only magnetic moment survives in all cases and is related to the total number of unpaired electrons. The magnetic moment of the Mn(III) derivative (1) was obtained on a solid sample at room temperature. For this compound, the magnetic value ( $\mu_{\text{eff}} = 4.96 \mu_B$ ) is comparable with that of other high-spin octahedral Mn(III) compounds [58]. The spin-only ( $g = 2$ ) value for  $S = 2$  is  $3.00 \text{ cm}^3 \text{ K mol}^{-1}$ .

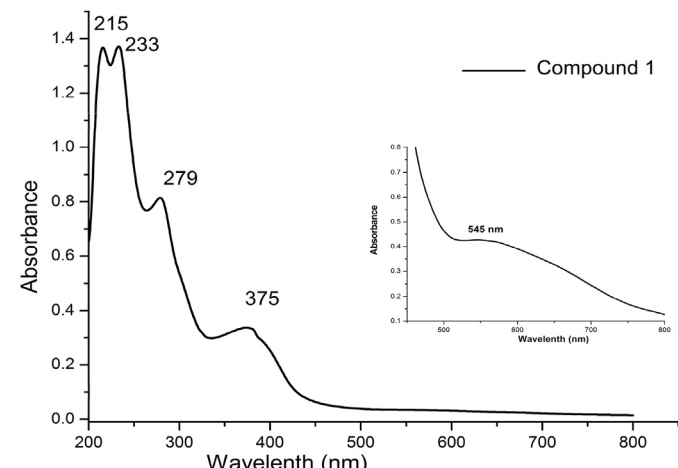


**Fig. 4.** Electronic spectrum of compound 1, measured in methanol.

has been demonstrated [62,63]. In DMSO and MeOH solution an identical behavior of 1 was revealed and no EPR signals could be detected (Fig. S3). These results would suggest that the elongated octahedral structure and +III oxidation state of 1 are retained in an organic solvent.

## 2.6. DFT studies

The theoretical study here reported is devoted to the analysis of the H-bonding network observed in the solid state of compound 1,

first elucidated through X-ray diffraction on single crystals (see Section 2.2 and Fig. 2). Particularly, we have studied and compared two H-bonded dimers involving either the Mn-coordinated water molecule or the hydroxyl group of the Schiff-base ligand. First of all, we have computed the molecular electrostatic potential (MEP) plotted onto the van der Waals surface (isosurface 0.001 a.u.) of compound 1 (Fig. 5) in order to investigate the electron rich and electron poor regions of the molecule. Two different orientations are represented in Fig. 5 and it can be observed that the most positive region is located at the OH group of the Schiff-base ligand (+65 kcal/mol, Fig. 5a). The MEP is also large and positive at the coordinated water molecule (+50 kcal/mol, Fig. 5a) probably due to its coordination to Mn. The most negative region is located in the middle of both the O-atoms of the ligand (-52 kcal/mol, Fig. 5b).

Moreover, the MEP is also large and negative (-44 kcal/mol, Fig. 5b) at the SCN ligand. Therefore, the most favoured interactions from an electrostatic point of view are H-bonds between the OH/H<sub>2</sub>O groups as donors and the O-atoms of the ligand and SCN as acceptors. Fig. 6a shows a partial view of the X-ray crystal structure of compound 1 (H-atoms omitted) where the two infinite 1D chains are represented. Two H-bonded dimers are highlighted, which are important connecting the 1D polymeric chains. The dimer denoted as "A" is self-assembled (Fig. 6b) where each coordinated water molecule establishes a bifurcated non-symmetrical H-bonding interactions with the two phenolic O-atoms of the Schiff-base ligand (blue and black dashed lines), O1W-H1W...O2<sup>ii</sup> and O1W-H1W...O3<sup>ii</sup>, respectively; ii = 2-x, y, 3/2-z. The interaction energy of this dimer is very large ( $\Delta E_1 = -29.9$  kcal/mol) due to the formation of these four electrostatically enhanced H-bonds, as suggested by the MEP surface in Fig. 5. Moreover, other long range interactions ( $\pi-\pi$  stacking) contributing to the interaction energy are also present in this dimer, as further commented below. In dimer B (Fig. 6c) the OH group forms a bifurcated H-bond with the phenolic O-atoms, in good agreement with the MEP analysis (see also Fig. 2: O1-H1...O2<sup>i</sup> and O1-H1...O3<sup>i</sup>; i = x, -y, -1/2 + z). Interestingly, in this dimer the H-atoms of the aliphatic linker interact with the  $\pi$ -system of the SCN ligand, thus establishing unconventional C-H... $\pi$ (SCN) interactions (C1<sup>iii</sup>-H1B<sup>iii</sup>...S1, C1<sup>iii</sup>-H1B<sup>iii</sup>...C18 and C2<sup>iii</sup>-H2<sup>iii</sup>...N3; iii = x, -y, 1/2+z). This agrees well with the MEP analysis that shows positive MEP values at these H-atoms (Fig. 5a) and negative at the thiocyanate ligand. The combination of both interactions [H-bonds and C-H... $\pi$ (SCN)] explains the large interaction energy computed for this dimer, i.e.

$\Delta E_2 = -23.4$  kcal/mol. Finally, in order to estimate the contribution of the C-H... $\pi$ (SCN) interaction we have computed an additional theoretical model where we have replaced the SCN ligand by a hydrido ligand (Fig. 6d). As a result, the interaction energy is reduced to  $\Delta E_3 = -20.3$  kcal/mol thus indicating that the contribution of the C-H... $\pi$ (SCN) interaction is modest (-3.1 kcal/mol).

In order to further characterize the non-covalent interactions commented above, we have used the NCI plot index computational tool. Non-covalent interactions are efficiently visualized and identified by using the NCI plot tool. It allows an easy assessment of host-guest complementarity and the extent to which weak interactions stabilize a complex. The color scheme is a red-yellow-green-blue scale with red for  $\rho_{\text{cut}}^+$  (repulsive) and blue for  $\rho_{\text{cut}}^-$  (attractive). Yellow and green surfaces correspond to weak repulsive and weak attractive interactions, respectively. The NCI plot of the dimer A of compound 1 is represented in Fig. 7a. The short (stronger) H-bond is characterized by a small and blue isosurface located between the O and the H atoms and the longer H-bond is characterized by a green isosurface. The NCI plot also reveals the presence of more extended isosurfaces between the aromatic rings, thus indicating the existence of  $\pi-\pi$  stacking interactions in this dimer that further stabilize the assembly. The NCI plot of the dimer B is represented in Fig. 7b. Similarly to dimer A, the bifurcated H-bond is characterized by one blue and one green isosurfaces located between the hydroxyl group and the O-atoms. In addition, the NCI plot shows a more extended and green isosurface that is located between the SCN ligand and two aliphatic H-atoms of the Schiff base ligand thus confirming the existence of the unconventional C-H... $\pi$ (SCN) interaction. Finally, the intramolecular HB is characterized by a small and blue isosurface.

### 3. Conclusion

A new Mn(III) derivative has been synthesized by employing a N<sub>2</sub>O<sub>3</sub> donor Schiff base precursor, [N,N'-bis(salicylaldehyde)-1,3-diaminopropan-2-ol], H<sub>2</sub>L. The solid state structure of 1 reveals that the Mn<sup>III</sup> atom possesses an octahedral environment based on the N<sub>2</sub>O<sub>2</sub> donor atoms of the ligand and on the coordination of a water molecule and an SCN<sup>-</sup> anion. The EPR spectroscopy carried out both in the solid state and in different solvents (DMSO and CH<sub>3</sub>OH) confirms the +3 oxidation state of the Mn ion. Compound 1 self assembles into a 2D network structure via O-H...O,  $\pi-\pi$ , and unconventional C-H... $\pi$ (SCN) interactions involving the  $\pi$ -system of the thiocyanate. DFT studies combined with MEP and NCI plots have been used to characterize and rationalize the interactions that are energetically very favorable due to the enhanced acidity of the H-bond donors and the anionic nature of the acceptors. Further exploration on electrocatalytic water oxidation studies utilizing this Mn<sup>III</sup> derivative is in progress in our laboratory.

### 4. Experimental section

#### 4.1. Materials

All the experiments were carried out under aerobic conditions. MnCl<sub>2</sub>·4H<sub>2</sub>O was purchased from Aldrich Chemicals. Salicylaldehyde, 1,3-diamino-2-propanol and sodium thiocyanate were purchased from Merck, India. Solvents were of reagent grade and used without further purification. The Schiff base precursor was prepared according to the literature [48].

#### 4.2. Physical measurements

Microanalytical data (C, H, and N) were collected on a Perkin-Elmer 2400 CHNS/O elemental analyzer. FTIR spectra were

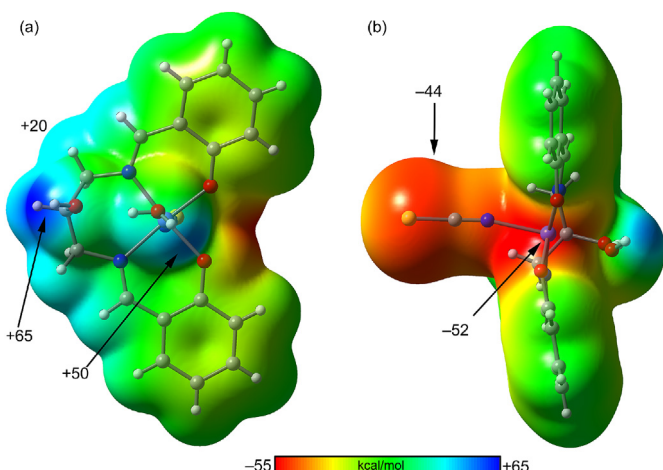
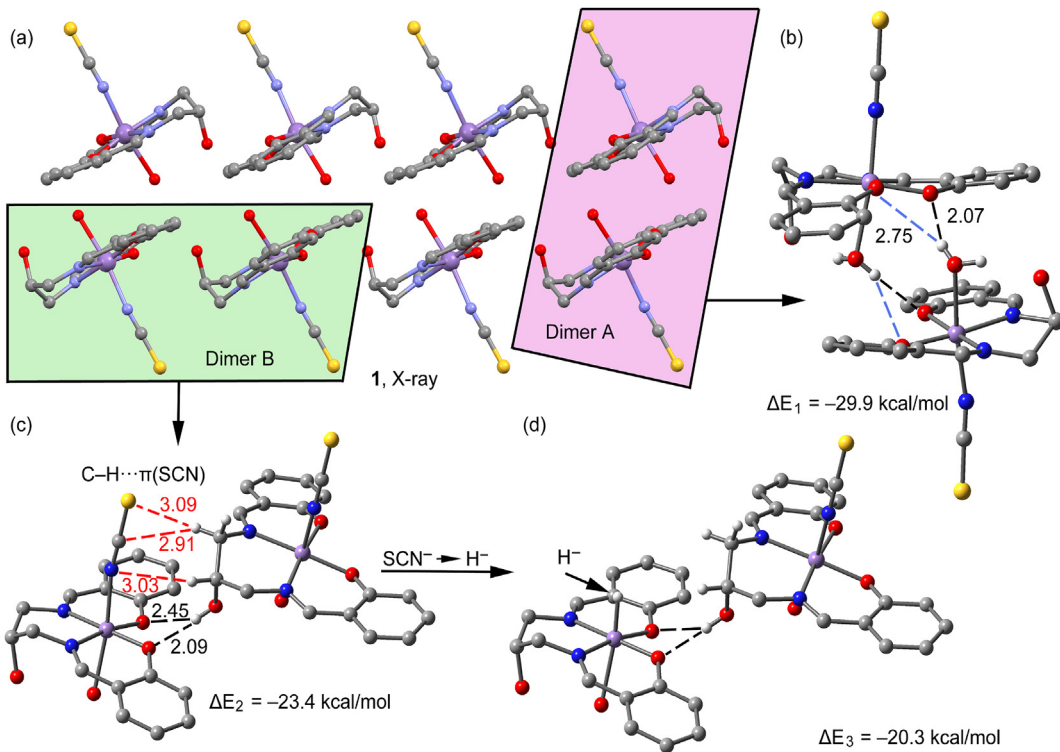
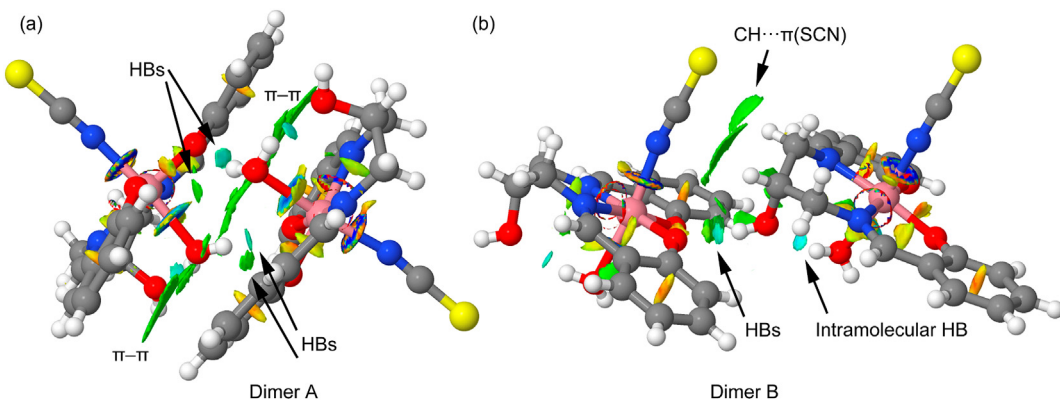


Fig. 5. Two views of the MEP surface of a model of compound 1. The values at selected points of the surface are indicated.



**Fig. 6.** (a) Partial view of the X-ray crystal structure of compound 1. H-atoms have been omitted for clarity. (b–d) Theoretical models used to evaluate the noncovalent interactions. Distances in Å. H-atoms have been omitted for clarity apart from those participating in H-bonding interactions.



**Fig. 7.** NCI plots of the dimers A (a) and B (b). The gradient cut-off is  $s = 0.35 \text{ au}$ , and the color scale is  $-0.04 < \rho < 0.04 \text{ au}$ .

recorded on a PerkinElmer RX-1 spectrophotometer in the range 3600–450 cm<sup>-1</sup> as KBr pellets. Electronic spectra were measured on a PerkinElmer Lambda 25 (U.V.–Vis.–N.I.R.) spectrophotometer. EPR spectra were recorded from 0 to 8000 Gauss in the temperature range 100–298 K on the polycrystalline powder and at 100 K on the polycrystalline powder dissolved in DMSO or MeOH with an X-band Bruker EMX spectrometer equipped with a HP 53150A microwave frequency counter. The instrumental parameters were as follows: microwave frequency, 9.40–9.41 GHz; microwave power, 20 mW; time constant, 81.92 ms; modulation frequency, 100 kHz; modulation amplitude, 0.4 mT; resolution, 4096 points. Room temperature magnetic susceptibilities were measured with the 155 PAR vibrating sample magnetometer fitted with a Waker Scientific 175 FBAL magnet.

#### 4.3. Synthesis of the ligand ( $H_2L$ )

First a 30 mL methanol solution of salicyldehyde (30 mmol, 3.66 g) was added to a 15 mL methanol solution of 1,3-diamino-2-propanol (15 mmol, 1.35 g). The resulting orange solution was then refluxed for 1 h, and after cooling down, the solvent was removed under reduced pressure to afford an orange crystalline solid which was collected as the ligand. Yield: 69%. Anal. Calc. for C<sub>17</sub>H<sub>18</sub>N<sub>2</sub>O<sub>3</sub>: C, 68.42; H, 6.09; N, 9.39. Found: C, 68.77; H, 5.73; N, 9.71%.

#### 4.4. Synthesis of compound (1)

To a methanol solution (10 mL) of MnCl<sub>2</sub>·4H<sub>2</sub>O (0.197 g, 1 mmol), H<sub>2</sub>L (1 mmol) in 15 mL of methanol was added under constant stirring. The resulting green solution was kept boiling for

10 min. After that, still in warm condition, a 10 mL water solution of sodium thiocyanate (0.081 g, 1 mmol) was added and the mixture was kept undisturbed at room temperature. Dark brown rectangular-shaped single crystals of 1 were generated after one week. These were separated by filtration and air-dried before carrying out all physical measurements and analyses. Yield: 0.71 g. Anal. Calc. for  $C_{18}H_{18}O_4N_3SMn$ : C, 50.42; H, 4.47; N, 9.80. Found: C, 50.11; H, 4.71; N, 9.57%.

#### 4.5. X-ray crystallography

The crystal structure of compound 1 was determined by X-ray diffraction methods. Intensity data and cell parameters were recorded at 293(2) K on a Bruker Breeze diffractometer ( $MoK\alpha$  radiation  $\lambda = 0.71073 \text{ \AA}$ ) equipped with a CCD area detector and a graphite monochromator. The raw frame data were processed using the programs SAINT and SADABS to yield the reflection data file [64]. The structure was solved by Direct Methods using the SIR97 program [65] and refined on  $F^2$  by full-matrix least-squares procedures, using the SHELXL-2014/7 program [66] in the WinGX suite v.2014.1 [67]. All non-hydrogen atoms were refined with anisotropic atomic displacements, while the H atoms bound to C and O were placed in calculated positions and refined isotropically using the riding model, with C–H distances ranging from 0.93 to 0.98  $\text{\AA}$ , O–H = 0.82  $\text{\AA}$  and  $U_{iso}(H)$  set to 1.2–1.5  $U_{eq}(C/O)$ . The H atoms of the water molecule were found in the difference Fourier map and refined freely. The weighting scheme used in the last cycle of refinement was  $w = 1/[\sigma^2 F^2 + (0.0514P)^2 + 8.6151P]$ , where  $P = (F^2 + 2F_c^2)/3$ . Crystal data and experimental details for data collection and structure refinement are reported in Table 3. Crystallographic data for the structure reported have been deposited with the Cambridge Crystallographic Data Centre as supplementary publication no. CCDC-1907942 and can be obtained free of charge on application to the CCDC, 12 Union Road, Cambridge, CB2 1EZ, UK (fax: +44-1223-336-033; e-mail [deposit@ccdc.cam.ac.uk](mailto:deposit@ccdc.cam.ac.uk) or <http://www.ccdc.cam.ac.uk>).

#### 4.6. Theoretical methods

The calculations of the noncovalent interactions and molecular electrostatic potential (MEP) surfaces were carried out using the Gaussian-09 program [68] and the B3LYP-D/def2-TZVP level of theory. Grimme's dispersion correction has been used in the

**Table 3**  
Crystallographic data of compound 1.

Empirical formula	$C_{18}H_{18}O_4N_3SMn$
Formula weight	427.35
Temperature	293(2)
Wavelength ( $\text{\AA}$ )	0.71073
Crystal system	Monoclinic
Space group	$C2/c$
$a, \text{\AA}$	21.588(8)
$b, \text{\AA}$	14.338(5)
$c, \text{\AA}$	14.719(5)
$\beta, \text{deg}$	124.524(4)
Volume, $\text{\AA}^3$	3754(2)
$Z$	8
$D_{\text{calc}} (\text{mg m}^{-3})$	1.512
$\mu (\text{Mo K}\alpha) (\text{mm}^{-1})$	0.844
$F(000)$	1760
Total reflections	18086
Unique reflections ( $R_{\text{int}}$ )	3158 (0.0606)
Observed reflections [ $F_o > 4\sigma(F_o)$ ]	2382
GOF on $F^2$	1.002
$R$ indices [ $F_o > 4\sigma(F_o)$ ] $R_1$ , $wR_2$	0.0456, 0.1050
Largest diff. peak and hole, $e.\text{\AA}^{-3}$	0.583, -0.369

calculations [69]. To evaluate the interactions in the solid state, the crystallographic coordinates were used and only the position of the H-bonds has been optimized. This procedure and theoretical method have been successfully used in the past to evaluate similar interactions [40,41,70]. The interaction energies were computed by calculating the difference between the energies of the isolated monomers and their assembly. The NCI plot is a visualization index that efficiently allows the identification and visualization of non-covalent interactions [71]. It is based on the electron density and its derivatives and the isosurfaces correspond to both favorable and unfavorable interactions. They are easily differentiated by the sign of the second density Hessian eigenvalue and defined by the isosurface color. NCI analysis is a very convenient tool to rationalize host–guest complementarity and to know which interactions stabilize a complex. The color scheme is a red-yellow-green-blue scale with red for  $\rho_{\text{cut}}^+$  (repulsive) and blue for  $\rho_{\text{cut}}^-$  (attractive). Yellow and green surfaces correspond to weak repulsive and weak attractive interactions, respectively [72]. The molecular electrostatic potential surfaces were computed at the same level using the G09 program and plotted using the Gaussview software.

#### Statement

We wish to assure that our manuscript does not contain any potential interest or “no conflict of interest”.

#### Acknowledgments

KD expresses her appreciation to the SERB (Science and Engineering Research Board, India) Grant (PDF/2016/002832) for financial assistance. AF wish to thank the DGICYT of Spain (project CTQ2017-85821-R FEDER funds). We also thank the CTI (UIB) for computational facilities.

#### Appendix A. Supplementary data

Supplementary data to this article can be found online at <https://doi.org/10.1016/j.molstruc.2019.126985>.

#### References

- V.L. Pecoraro (Ed.), Manganese Redox Enzymes, VCH, New York, 1992.
- G. Christou, Acc. Chem. Res. 22 (1989) 328–335.
- L. Que, A.E. True, Prog. Inorg. Chem. 38 (1990) 97–200.
- K. Sauer, Acc. Chem. Res. 13 (1980) 249–256.
- Govindjee, W. Coleman, Sci. Am. 260 (1990) 50–58.
- G. Renger, Angew. Chem. Int. Ed. Engl. 26 (1987) 643–660.
- P. Zanello, S. Tamburini, P.A. Vigato, G.A. Mazzocchin, Coord. Chem. Rev. 77 (1987) 165–273.
- M.D. Timken, W.A. Marrit, D.N. Hendrickson, R.R. Gagne, E. Sinn, Inorg. Chem. 24 (1985) 4202–4209.
- O. Pouralimardan, A.C. Chamayou, C. Janiak, H.M. Hassan, Inorg. Chem. Acta 360 (2007) 1599–1608.
- R.H. Holm, G.W. Everett Jr., A. Chakravorty, Prog. Inorg. Chem. 7 (1966) 83–214.
- J.P. Costes, F. Dahan, J.M. Dominguez-Vera, J.P. Laurent, J. Ruiz, J. Sotiropoulos, Inorg. Chem. 33 (1994) 3908–3913.
- J.L. Sessler, J.W. Sibert, V. Lynch, J.T. Markert, C.L. Wooten, Inorg. Chem. 32 (1993) 621–626.
- G.W. Inman Jr., W.E. Hatfield, Inorg. Chem. 11 (1972) 3085–3090.
- P.A. Vigato, S. Tamburini, D.E. Fenton, Coord. Chem. Rev. 106 (1990) 25–170.
- A.D. Gamovskii, A.L. Nivorozhkin, V.I. Minkin, Coord. Chem. Rev. 126 (1993) 1–69.
- E.K. Pistorius, G.H. Schmid, Biochem. Biophys. Acta 890 (1987) 352–359.
- K.P. Bader, P. Thibault, G.H. Schmid, Z. Naturforschung 38 (1983) 778–792.
- H.-L. Shyu, H.-H. Wei, Y. Wang, Inorg. Chim. Acta 290 (1999) 8–13.
- Y. Cringh, S.W. Gordon-Wylie, R.E. Norman, G.R. Clark, S.T. Weintraub, C.P. Horwitz, Inorg. Chem. 36 (1997) 4968–4974.
- M. Verdaguier, A. Bleuzen, V. Marvaud, J. Vaissermann, M. Seuleiman, C. Desplanches, A. Scuiller, C. Train, R. Garde, G. Gelly, C. Lomenech, I. Rosenman, P. Veillet, C. Cartier, F. Villain, Coord. Chem. Rev. 190–192 (1999) 1023–1047.

- [21] C. Mathoniere, J.-P. Sutter, J.V. Yakhmi, in: J.S. Miller, M. Drillon (Eds.), *Magnetism: Molecules to Materials* vol. 4, VCH, Weinheim, 2002, pp. 1–40.
- [22] H. Miyasaka, R. Clérac, T. Ishii, H.-C. Chang, S. Kitagawa, M. Yamashita, *J. Chem. Soc., Dalton Trans.* (2002) 1528–1534.
- [23] O. Kahn, *Molecular Magnetism*, VCH, Weinheim, Germany, 1993.
- [24] S.K. Dey, N. Mondal, M.S. El Fallah, A. Escuer, X. Solans, T. Matsushita, V. Gramlich, S. Mitra, *Inorg. Chem.* 43 (2004) 2427–2434.
- [25] K.R. Reddy, M.V. Rajasekharan, J.P. Tuchagues, *Inorg. Chem.* 37 (1998) 5978–5982.
- [26] H. Li, Z.J. Zhong, C.Y. Duan, X.Z. You, T.C.W. Mak, B. Wu, *Inorg. Chim. Acta* 271 (1998) 99–104.
- [27] B.R. Stults, R.S. Marianelli, V.W. Day, *Inorg. Chem.* 14 (1975) 722–730.
- [28] B.R. Stults, R.O. Day, R.S. Marianelli, V.W. Day, *Inorg. Chem.* 18 (1979) 1847–1852.
- [29] R. Inglis, F. White, S. Piligkos, W. Wernsdorfer, E.K. Brechin, G.S. Papaefstathiou, *Chem. Commun.* (2011) 3090–3092.
- [30] V. Kotzabasaki, R. Inglis, M. Siczek, T. Lis, E.K. Brechin, C.J. Milius, *Dalton Trans.* (2011) 1693–1699.
- [31] Y. Zheng, X.-J. Kong, L.-S. Long, R.-B. Huang, L.-S. Zheng, *Dalton Trans.* (2011) 4035–4037.
- [32] P.-P. Yang, X.-L. Wang, L.-C. Li, Di-Z. Liao, *Dalton Trans.* (2011) 4155–4161.
- [33] M. Manoli, R. Inglis, M.J. Manos, V. Nastopoulos, W. Wernsdorfer, E.K. Brechin, A.J. Tasiopoulos, *Angew. Chem. Int. Ed.* 50 (2011) 4441–4444.
- [34] S. Wang, L. Kong, H. Yang, Z. He, Z. Jiang, D. Li, S. Zeng, M. Niu, Y. Song, J. Dou, *Inorg. Chem.* 50 (2011) 2705–2707.
- [35] P. Talukder, A. Datta, S. Mitra, G.M. Rosair, M.S. El Fallah, J. Ribas, *Dalton Trans.* (2004) 4161–4167.
- [36] K. Das, A. Datta, S. Nandi, S.B. Mane, S. Mondal, C. Massera, C. Sinha, C.-H. Hung, T. Askun, P. Celikboyun, Z. Cantürk, E. Garribba, T. Akitsu, *Inorg. Chem. Frontier* 2 (2015) 749–762.
- [37] A. Datta, K. Das, C. Massera, J.K. Clegg, C. Sinha, J.-H. Huang, E. Garribba, *Dalton Trans.* 43 (2014) 5558–5563.
- [38] A. Datta, K. Das, S.B. Mane, S. Mendiratta, M.S. El Fallah, E. Garribba, A. Bauza, A. Frontera, C.-H. Hung, C. Sinha, *RSC Adv.* 6 (2016) 54856–54865.
- [39] K. Das, A. Datta, S. Roy, J.K. Clegg, E. Garribba, C. Sinha, H. Kara, *Polyhedron* 78 (2014) 62–71.
- [40] K. Das, S. Goswami, B.B. Beyene, A.W. Yibeltal, E. Garribba, A. Frontera, A. Datta, *Polyhedron* 159 (2019) 323–329.
- [41] K. Das, A. Datta, S. Mendiratta, E. Garribba, A. Frontera, Z. Cantürk, *J. Mol. Struct.* 1175 (2019) 948–955.
- [42] M.S. Ray, A. Ghosh, R. Bhattacharya, G. Mukhopadhyay, M.G.B. Drew, J. Ribas, *Dalton Trans.* (2004) 252–259.
- [43] M.S. Ray, S. Chattopadhyay, M.G.B. Drew, A. Figueroa, J. Ribas, C. Diaz, A. Ghosh, *Eur. J. Inorg. Chem.* (2005) 4562–4571.
- [44] P. Mukherjee, C. Biswas, M.G.B. Drew, A. Ghosh, *Polyhedron* 26 (2007) 3121–3128.
- [45] P. Mukherjee, M.G.B. Drew, A. Ghosh, *Inorg. Chem.* 48 (2009) 2364–2370.
- [46] M.J. MacLachlan, M.K. Park, L.K. Thompson, *Inorg. Chem.* 35 (1996) 5492–5499.
- [47] X. Lu, W.-Y. Wong, W.-K. Wong, *Eur. J. Inorg. Chem.* (2008) 523–528.
- [48] F. Brezina, Z. Smekal, Z. Travnicek, Z. Sindelar, R. Pastorek, J. Marek, *Polyhedron* 16 (1997) 1331–1336.
- [49] K. Nakamoto, *Infrared and Raman Spectra of Inorganic and Coordination Compounds*, vol. 23, Wiley, New York, 1997.
- [50] S.H. Rahaman, R. Ghosh, T.H. Lu, B.K. Ghosh, *Polyhedron* 24 (2005) 1525–1532.
- [51] R.T. Conley, *Infrared Spectroscopy*, Allyn & Bacon, Boston, 1966.
- [52] Z.L. You, H.L. Zhu, *Z. Anorg. Allg. Chem.* 630 (2004) 2754–2760.
- [53] I.S. Antonijević, G.V. Janjić, M.K. Milčić, S.D. Žarić, *Cryst. Growth Des.* 16 (2016) 632–639.
- [54] A.B.P. Lever, *Inorganic Electronic Spectroscopy*, Elsevier Science, New York, 1984.
- [55] M. Maiti, D. Sadhukhan, S. Thakurta, E. Zangrando, G. Pilet, A. Bauzá, A. Frontera, B. Dede, S. Mitra, *Polyhedron* 75 (2014) 40–49.
- [56] S. Sen, P. Talukder, S.K. Dey, S. Mitra, G. Rosair, D.L. Hughes, G.P.A. Yap, G. Pilet, V. Gramlich, T. Matsushita, *Dalton Trans.* (2006) 1758–1767.
- [57] K. Das, A. Datta, B.B. Beyene, C. Massera, E. Garribba, C. Sinha, T. Akitsu, S. Tanka, *Polyhedron* 127 (2017) 315–322.
- [58] R.L. Dutta, A. Syamal, in: *Elements of Magnetochemistry*, S Chand & Company Ltd., New Delhi, India, 1982.
- [59] R.S. Drago, *Physical Methods in Chemistry* W. B. Saunders Company, Philadelphia, 1977.
- [60] F.E. Mabbas, D. Collison, *Electron Paramagnetic Resonance of D Transition Metal Compounds*, Elsevier Science Publishers B.V., Amsterdam, 1992.
- [61] B.R. McGarvey, in: R.L. Carlin (Ed.), *In Transition Met. Chem.* (London), vol. 3, Marcel Dekker, New York, 1966, pp. 89–201.
- [62] K.A. Campbell, M.R. Lashley, J.K. Wyatt, M.H. Nantz, R.D. Britt, *J. Am. Chem. Soc.* 123 (2001) 5710–5719.
- [63] I. Syiemlieh, A. Kumar, S.D. Kurbah, A.K. De, R.A. Lal, *J. Mol. Struct.* 1151 (2018) 343–352.
- [64] (a) SADABS Bruker AXS, 2004. Madison, Wisconsin, USA;  
 (b) SAINT, Software Users Guide, Version 6.0; Bruker Analytical X-Ray Systems, 1999. Madison, WI;  
 (c) G.M. Sheldrick, SADABS v2.03: Area-Detector Absorption Correction, University of Göttingen, Germany, 1999.
- [65] A. Altomare, M.C. Burla, M. Camalli, G.L. Cascarano, C. Giacovazzo, A. Guagliardi, A.G.G. Moliterni, G. Polidori, R. Spagna, *J. Appl. Crystallogr.* 32 (1999) 115–119.
- [66] G.M. Sheldrick, *Acta Crystallogr. A* A64 (2008) 112–122.
- [67] L.J. Farrugia, *J. Appl. Crystallogr.* 45 (2012) 849–854.
- [68] M.J. Frisch, G.W. Trucks, H.B. Schlegel, G.E. Scuseria, M.A. Robb, J.R. Cheeseman, G. Scalmani, V. Barone, G.A. Petersson, H. Nakatsuji, X. Li, M. Caricato, A. Marenich, J. Bloino, B.G. Janesko, R. Gomperts, B. Mennucci, H.P. Hratchian, J.V. Ortiz, A.F. Izmaylov, J.L. Sonnenberg, D. Williams-Young, F. Ding, F. Lipparini, F. Egidi, J. Goings, B. Peng, A. Petrone, T. Henderson, D. Ranasinghe, V.G. Zakrzewski, J. Gao, N. Rega, G. Zheng, W. Liang, M. Hada, M. Ehara, K. Toyota, R. Fukuda, J. Hasegawa, M. Ishida, T. Nakajima, Y. Honda, O. Kitao, H. Nakai, T. Vreven, K. Throssell, J.A. Montgomery Jr., J.E. Peralta, F. Ogliaro, M. Bearpark, J.J. Heyd, E. Brothers, K.N. Kudin, V.N. Staroverov, T. Keith, R. Kobayashi, J. Normand, K. RagHAVACHARI, A. Rendell, J.C. Burant, S.S. Iyengar, J. Tomasi, M. Cossi, J.M. Millam, M. Klene, C. Adamo, R. Cammi, J.W. Ochterski, R.L. Martin, K. Morokuma, O. Farkas, J.B. Foresman, D.J. Fox, Gaussian, Inc., Wallingford CT, 2016.
- [69] S. Grimme, J. Antony, S. Ehrlich, H. Krieg, *J. Chem. Phys.* 132 (2010) 154104–154119.
- [70] K. Das, G.W. Woyessa, A. Datta, B.B. Beyene, S. Goswami, E. Garribba, A. Frontera, C. Sinha, *J. Mol. Struct.* 1173 (2018) 462–468.
- [71] J. Contreras-García, E.R. Johnson, S. Keinan, R. Chaudret, J.-P. Piquemal, D.N. Beratan, W. Yang, *J. Chem. Theory Comput.* 7 (2011) 625–632.
- [72] E.R. Johnson, S. Keinan, P. Mori-Sánchez, J. Contreras-García, A.J. Cohen, W. Yang, *J. Am. Chem. Soc.* 132 (2010) 6498–6506.